Bond Orientation Decay and Stress Relaxation in a Model Polymer Melt

Jianping Gao

School of Physics, Georgia Institute of Technology, Atlanta, Georgia 30332-0430

Jerome H. Weiner*

Division of Engineering, Brown University, Providence, Rhode Island 02912

Received February 12, 1996; Revised Manuscript Received May 13, 1996[⊗]

ABSTRACT: Simulations of stress relaxation in a model polymer melt of freely-jointed chains with $N = 300$ bonds are performed with the use of a nonequilibrium molecular dynamics algorithm. After a deformation is applied in a short loading period, special attention is paid to the decay of bond orientation, $P_2(t;1)$, and the relation of this quantity to the stress $\sigma(t)$ computed by the atomic virial stress formula. It is found that the ratio $P_2(t;1)/\sigma(t)$ has a low value in the early glassy period and then undergoes a transition to a higher value that remains substantially constant. An explanation on the atomic level for the behavior of this ratio, which bears a close relation to the stress-optical coefficient is given. Various modes of coarse-graining the model melt are considered by subdivision of each chain into segments, each with N_R bonds. A second, molecular, calculation of the stress is made for the coarse-grained melt by use of the entropic spring stress formula and denoted by $\sigma_e(t;N_R)$. At early times $\sigma(t) > \sigma_e(t;N_R)$ for all N_R. At later times, the value of N_R for which $\sigma(t) = \sigma_e(t;N_R)$ increases from $N_R = 5$ to $N_R = 50$. In these simulations, no value of N_R is found for which $\sigma = \sigma_e$ for an extended period. Conceptual difficulties, suggested by these simulations, with the use of Rouse dynamics for the calculation of the plateau onset and plateau modulus are discussed.

1. Introduction

The concept of reptation[1] has played a central role for the past 20 years in the study of stress relaxation in polymer melts and has been used by Doi and Edwards[2,3] in their widely studied analytical theory of the process. Much effort, both experimental[4−8] and based on computer simulation,[9−15] has gone into the determination of whether chain motion does indeed occur by reptation. An excellent review is given by Lodge *et al.*[16] Important as this question is, it is only part of the story. In addition, even if the motion of all monomers is regarded as known, it is still necessary to compute the time evolution of the stress due to this motion. This step is accomplished in most theories, including that of Doi and Edwards, by regarding the chains as each composed of a number of segments, with each segment long enough to be regarded as a linear entropic spring. The stress is then taken as due solely to the tension in these springs; interchain interactions, in particular excluded volume interactions, are assumed to make only a hydrostatic contribution. We refer to this approach as the entropic spring stress formulation (ESSF).

We have been conducting computer simulation studies of the stress relaxation process by use of a nonequilibrium molecular dynamics (NEMD) algorithm[17−19] and computing the time-dependent stress on an atomic basis by means of the atomic virial formula. In contrast to the molecular ESSF, on the atomic level we find, as we did in earlier equilibrium studies on networks,[20] that the deviatoric or anisotropic stress is due primarily to the excluded volume interactions. A similar conclusion for stress relaxation has been reached by Fixman,[21] using an equilibrium algorithm based on the Green−Kubo formula.

We regard the stress based on the atomic virial as the rigorously correct stress corresponding to the monomer motion as determined by molecular dynamics. The question then arises: For what portion, if any, of the stress relaxation process does the ESSF give the same result as the atomic virial? To our knowledge, there has been no theoretical treatment of this question. Our NEMD simulations show, as expected, that the atomic virial stress greatly exceeds that computed on the basis of the ESSF in the early stages of stress relaxation (glassy period). One of the questions we wish to focus on in this paper is whether the ESSF can be used in the period in which the transition to the plateau occurs. Our simulations are confined to the earlier period of stress relaxation, roughly up to twice the entanglement time τ_e.

We have also expanded our previous NEMD program to include the calculation of the bond orientation and its variation in time and along the chain length. This permits us to examine the following questions: Is the variation of bond orientation decay along the chain length consistent with motion by reptation? What is the relation of bond orientation decay to stress relaxation in the system?

We continue to use the freely-jointed chain model of ref 19, where details of the model and the NEMD algorithm may be found. For convenience, we summarize some of the salient features here. The bonded potential $u_b(r)$ is

$$u_b(r) = {}^1/_2\kappa(r - a)^2 \tag{1}$$

where r is the distance between adjacent atoms on a given chain and a is the zero-force bond length. The nonbonded potential $u_{nb}(r)$ is the repulsive part of a Lennard-Jones potential; that is

$$\begin{aligned} u_{nb}(r) &= 4\epsilon_{LJ}[(\sigma_{LJ}/r)^{12} - (\sigma_{LJ}/r)^6] \qquad \text{for } r \le r_0 \\ &= u_{nb}(r_0) \qquad \text{for } r \ge r_0 \end{aligned} \tag{2}$$

where r denotes the distance between any adjacent pair

[⊗] Abstract published in *Advance ACS Abstracts,* July 15, 1996.

S0024-9297(96)00217-3 CCC: $12.00

of atoms on a given chain or between any pair of atoms on different chains and $r_0 = 2^{1/6}\sigma_{LJ}$. The results reported in this paper are for parameter values $\sigma_{LJ} = a$, $\kappa a^2/kT_0 = 267$, and $\epsilon_{LJ}/kT_o = 1.0$. For these parameter values, the model approximates a chain of tangent hard spheres. We take the view here that we are dealing with an idealized model of a polymer chain and not a coarse-grained treatment of a realistic chain. That is, we regard adjacent particles or atoms on a given chain as representative of neighboring monomers on a real chain, and the bond between these atoms as representing the backbone covalent bond joining these monomers. The distinction is important, since one of the aims of this work is to study the effects of different degrees of coarse-graining of this idealized chain model and, by implication, the nature of the coarse-graining process when applied to real systems. Furthermore, we have found[20] that the bonds of this chain model in melts at the densities studied here are in compression throughout the unloading period; it would, therefore, be inconsistent to regard them as segments of a coarse-grained chain acting as entropic springs in tension. The fact that backbone bonds are in compression in melts of realistic density was observed as well in simulations of model melts with more realistic chain models, e.g., in simulations employing the polyethylene model studied extensively by Takeuchi and Roe.[22] The physical basis of this phenomenon has been given elsewhere.[23,29]

The simulation is carried out using periodic boundary conditions as is customary in molecular dynamics simulation. The basic cell, referred to a rectangular Cartesian coordinate system x_1,x_2,x_3, is a rectangular parallelepiped with dimensions in the coordinate directions at time t, $L_1(t),L_2(t),L_3(t)$. At time $t = 0$, $L_1 = L_2 = L_3 = L$, and the cell is subjected, for $0 \le t \le t_1$, to a constant-volume, constant-strain-rate (referred to current dimensions) elongation, $\dot\epsilon$, in the x_1 direction, and $-\dot\epsilon/2$ in the x_2 and x_3 directions. For $t > t_1$, the cell dimensions are held fixed. Interactions between atoms in the basic cell with image atoms across the cell wall serve to transmit the deformation to the atoms in the basic cell. In addition, a velocity increment corresponding to a velocity gradient equivalent to the constant-volume elongation at rate $\dot\epsilon$ is added to all the atom velocities at $t = 0$ and subtracted from the atom velocities at $t = t_1$. We refer to the period $0 \le t \le t_1$ as the loading period and to the period $t > t_1$ as the unloading period. In the time unit $(m\sigma_{LJ}^2/\epsilon_{LJ})^{1/2}$, where m is the atomic mass, $\dot\epsilon = 0.0327$, $t_1 = 15.3$, and the total simulated unloading time is 7000. The algorithm employed in the simulation[19] maintained a constant temperature in the system. The system pressure decreased about 2% during loading and then gradually returned to its original value upon unloading. In what follows, we focus on the unloading period in this paper and set $t = 0$ as the start of unloading.

The initial melt configuration is generated by the recently developed "polymerization" method of Gao[24] which leads rapidly to a well-equilibrated initial melt. For each set of parameters, we use 4 initial melt configurations, each generated independently, with the simulation for each initial configuration repeated 3 times, with permutation of the coordinate directions. There are, therefore, 12 separate simulations or trajectories. In addition to ensemble averaging over the 12 trajectories, we utilize time averaging over time intervals that increase in length so as to correspond to approximately equal spacing in log t. The results for each of the 12 trajectories are also computed separately and are used to obtain error bars for the ensemble-averaged values.

The molecular dynamics calculation yields the position of each atom of the model melt at each instant t of the loading and unloading period. As discussed earlier, the stress tensor in the melt is computed from these positions in two ways. The first is atom-based and utilizes the virial stress formula[17]

$$vt_{ij} = -nk_BT\delta_{ij} + \sum_{\alpha\in b}\langle r_\alpha^{-1}u'_b(r_\alpha)r_{\alpha i}r_{\alpha j}\rangle + \sum_{\alpha\in b}\langle r_\alpha^{-1}u'_{nb}(r_\alpha)r_{\alpha i}r_{\alpha j}\rangle \quad (3)$$

where v is the cell volume, t_{ij} are the components of the stress tensor (force per unit present area) referred to the fixed rectangular Cartesian system x_i ($i = 1, 2, 3$), n is the number of atoms per cell, δ_{ij} is the Kronecker delta, $\mathbf{r}_\alpha$ is the vector displacement between the α pair of atoms with components $r_{\alpha i}$, $r_\alpha = |\mathbf{r}_\alpha|$, $u_\alpha(r_\alpha)$ is the pair potential acting between the α pair, $u'_\alpha = du_\alpha/dr_\alpha$, brackets denote the ensemble average at time t over the 12 trajectories, and the notations $\alpha \in$ b or $\alpha \in$ nb indicate that the sums range over all pairs of bonded or nonbonded interacting atoms, respectively, with at least one atom of the pair in the basic cell. We are not interested in the entire stress tensor for this constant-volume process but only in its deviatoric or anisotropic portion. Equivalently, for the uniaxial extension deformation studied here, we can confine attention to the stress difference

$$\sigma(t) = t_{11}(t) - t_{22}(t) \quad (4)$$

The second method of stress calculation is molecular and based on the ESSF. Inherent in the use of the ESSF is a coarse-graining of the original system in which each chain is subdivided into ν_R subchains each with N_R bonds so that $\nu_R N_R = N$; we refer to each subchain as a segment.[25] The instantaneous end-to-end vector of an arbitrary segment β is denoted by $\mathbf{r}_\beta$ with components $r_{\beta i}$. The segment is assumed to act as a linear entropic spring with a tensile force whose components $f_{\beta i} = 3k_BTr_{\beta i}/(N_Ra^2)$. The corresponding stress tensor[26]

$$t_{ij}^e = \frac{1}{V}\sum_\beta \langle f_{\beta i}r_{\beta j}\rangle = \frac{3k_BT}{vN_Ra^2}\sum_\beta \langle r_{\beta i}r_{\beta j}\rangle \quad (5)$$

where the summation is carried out over all segments with at least one end in the basic cell. As in eq 4, we confine attention to the entropic stress difference, $\sigma_e(t)$, where

$$\sigma_e(t) = t_{11}^e(t) - t_{22}^e(t) = \frac{3k_BT}{vN_Ra^2}\sum_\beta \langle r_{\beta 1}^2 - r_{\beta 2}^2\rangle \quad (6)$$

Despite the difference in their appearance, the structures of eqs 3 and 5 may be seen to be the same, if we put aside the first term in eq 3, which does not contribute to the deviatoric stress in any case. The significant difference between the two methods of stress computation is that in the atomic virial, eq 3, the force is computed between all pairs of atoms on the basis of the appropriate interatomic potential, $u_b(r)$ or $u_{nb}(r)$; in the molecular ESSF, eq 5, the force is computed only between atoms at the ends of segments on the assumption that the segments are acting as linear entropic springs.

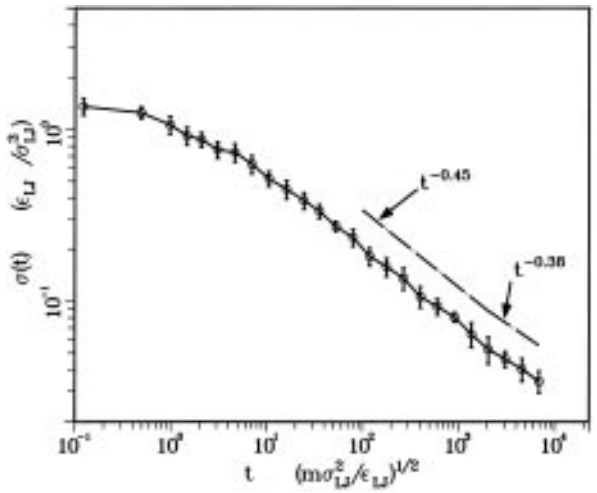

Figure 1. log−log plot of relaxation of stress difference $\sigma(t) = t_{11}(t) - t_{22}(t)$ for model polymer melt of freely-jointed chains with $N = 300$ bonds and reduced density $\rho = 1.0$, subjected initially to a constant-volume extension in the x_1 direction. Dash−dot straight lines show least-squares fits to $\sigma(t)$ during periods $10^2 < t < 2 \times 10^3$ ($\sigma(t) \sim t^{-0.45}$) and $2 \times 10^3 < t < 7 \times 10^3$ ($\sigma(t) \sim t^{-0.38}$).

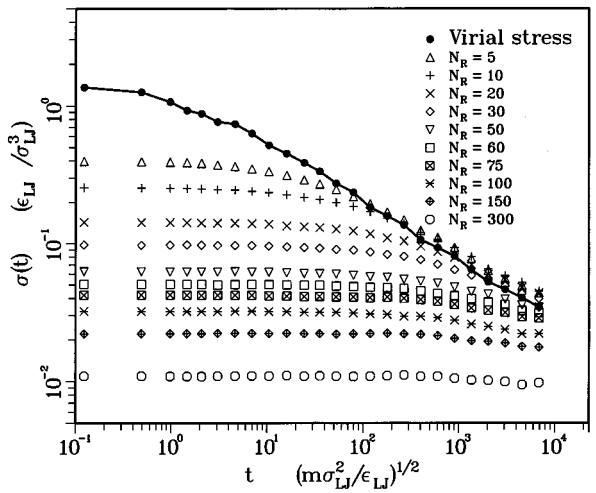

Figure 2. Comparison of $\sigma(t)$ (solid curve), stress difference computed on the basis of the atomic virial stress formula, eqs 3 and 4, and entropic stress difference $\sigma_e(t;N_R)$ computed on a molecular basis using the ESSF, eqs 5 and 6, for various values of N_R, the number of bonds per segment. Note that value of N_R for which $\sigma(t) = \sigma_e(t;N_R)$ goes from $N_R = 5$ at $t \cong 10^2$ to $N_R = 50$ at $t \cong 7 \times 10^3$.

The plan of this paper is as follows: An outline of the simulation results is presented in section 2. These are discussed in section 3 with special attention paid to the nature of bond orientation decay, to the relation between the atomic and molecular viewpoints, and to the utilization of Rouse dynamics in the transition regime. Finally, conclusions are summarized in section 4.

2. Simulation Results

An important parameter in the stress relaxation behavior of the melt is its reduced density, ρ, where

$$\rho = \frac{n\sigma_{LJ}{}^3}{v} \tag{7}$$

for a melt with n atoms in volume v. In these simulations for a melt of chains with $N = 300$ bonds, as in the previous study[19] for $N = 200$, we have concentrated our efforts on a melt with $\rho = 1.0$. The corresponding packing fraction $\varphi = (\pi/6)\rho = 0.52$. The entanglement length, N_e, for models similar to ours with $\rho = 0.85$ has been estimated in previous equilibrium simulations[10,15] as $N_e \cong 35$, although there is considerable uncertainty in this quantity. Since it appears[15] that N_e decreases with increasing ρ, these simulations for $\rho = 1.0$ and $N = 300$ should be well in the entanglement regime.

We show first, in Figure 1, the stress relaxation history as computed on the basis of the virial stress formula, eq 3. This figure also shows the error bars for the virial stress obtained from the results for the 12 trajectories regarded as independent simulations. The error bars for other computed quantities are generally of similar magnitude and are most times omitted for clarity.

The virial stress history, $\sigma(t)$, is repeated in Figure 2 together with the curves for $\sigma_e(t;N_R)$, the stress computed on the basis of eq 6, the ESSF based on segments with various values of N_R bonds. In order that a segment may be reasonably regarded as a linear entropic spring, a minimum value of $N_R = 5$ has been employed. The anomalous force−length behavior of segments with $N_R = 2$, 3, 4 has been shown, for example, in ref 27.

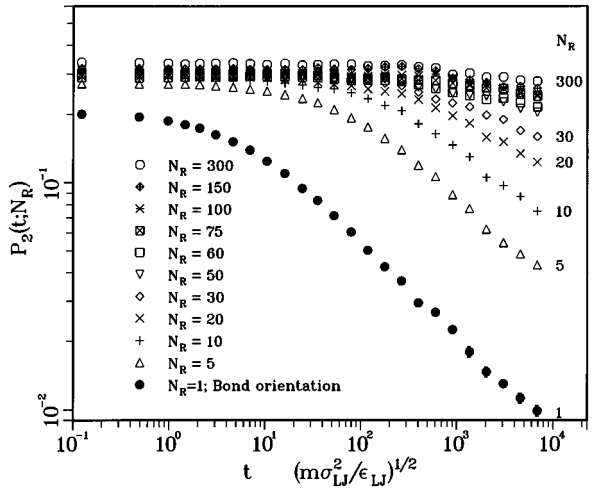

Figure 3. Decay of orientation measure $P_2(t;N_R)$, eq 8, for end-to-end vectors of segments with N_R bonds. The case of $N_R = 1$ corresponds to single-bond orientation decay. Error bars are included for the curve ($N_R = 1$), but since they are generally smaller than the symbol, they are visible only at a few of the later times.

As noted previously, the computer program for this work incorporates the computation of the quantities $P_2(t;N_R)$, where

$$P_2(t;N_R) = {}^1/_2(3\langle\cos^2\theta_R(t)\rangle - 1) \tag{8}$$

with $\theta_R(t)$ the angle with the x_1 axis made by the end-to-end vector of a segment with N_R bonds and where the ensemble average is taken over all such segments in all 12 trajectories. It is, therefore, a measure of the manner of the decay of the orientation of these segments originally introduced by the imposed deformation. The program also incorporates the corresponding quantity, denoted by $P_2(t;1)$, for the individual bonds of the chains. The results of these calculations of $P_2(t;N_R)$ for the various values of N_R are shown in Figure 3. It is seen that $P_2(t;1)$, the single-bond orientation decay history, is very similar in appearance to the decay of the virial stress $\sigma(t)$ shown in Figures 1 and 2 with, however, much smaller error bars. This similarity in $P_2(t;1)$ and $\sigma(t)$ is closely related to the stress optical law. We will

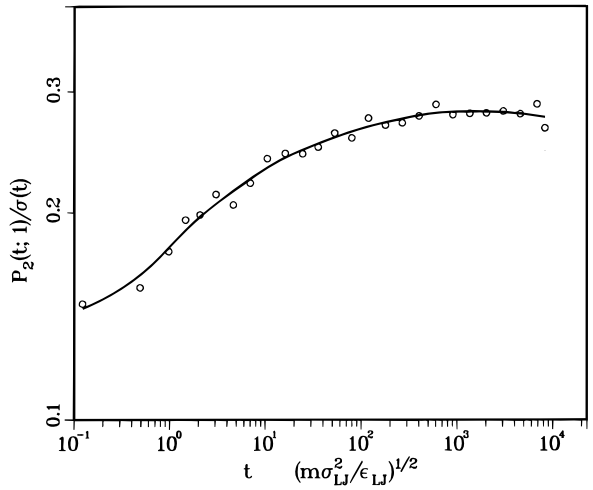

Figure 4. Ratio $P_2(t;1)/\sigma(t)$ where $P_2(t;1)$ is the orientation measure for the bonds in the melt. The solid curve is drawn to assist the eye.

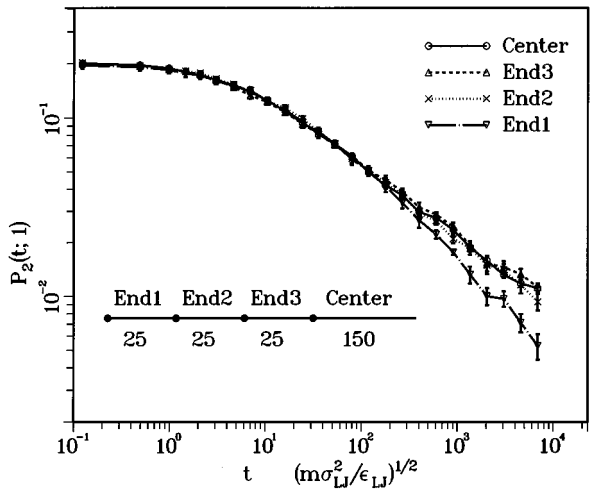

Figure 5. Variation of bond orientation decay along the chains. The curve labeled End1 is the average over the 25 bonds at the chain ends, End2 is the average over the next 25 bonds from the chain ends, End3 is the average over the next 25 bonds, and Center is the average over the central 150 bonds. The inset shows this subdivision for the left part of the chain; there is a corresponding subdivision of the 75 bonds at the right chain end.

discuss this question further in the following section and, in preparation, present in Figure 4 the ratio $P_2(t;1)/\sigma(t)$.

In the computation of the decay of bond orientation, averages are computed separately over the central portion of each chain and over end portions of the chain. The results are shown in Figure 5, where it is seen clearly that the decay of orientation over the central portions starts to slow down at $t \cong 10^2$ relative to the rate of decay of the end portion. The simulations also reveal that the contribution to $\sigma_e(t;N_R)$ by the chain ends decays more rapidly than the contribution from the central portion of the chain. As a typical example, the result for $N_R = 30$ is shown in Figure 6.

If, for a given coarse-graining corresponding to N_R, the monomers at segment ends during loading underwent the affine deformation and subsequently remained at those positions, then it follows from the affine theory of rubber elasticity that $\sigma_e(t;N_R)$ would be independent of t and proportional to N_R^{-1}. In order to compare the observed decay rates of $\sigma_e(t;N_R)$ as they depend on the value of N_R, they are replotted in Figure 7 as $N_R\sigma_e(t;N_R)$. The decay in $\sigma_e(t;N_R)$ is due both to the change in mean

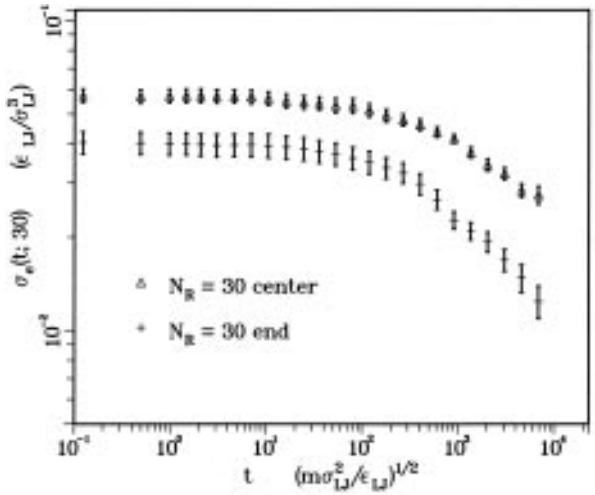

Figure 6. Contribution to the entropic stress $\sigma_e(t;30)$ made by the 6 segments in the center of chain and by the 2 portions at the chain ends consisting of 2 segments each.

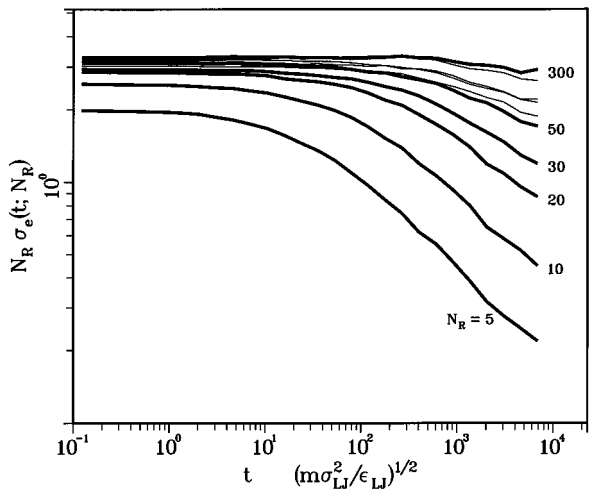

Figure 7. Decay rates of entropic stress $\sigma_e(t;N_R)$ for various values of N_R, the number of bonds per segment. Curves for $N_R = 60$, 75, 100, and 150 are not labeled and are represented by light curves for clarity; they appear in the expected sequence.

square length and in orientation of the segments. If the assumption is made that these two changes are uncorrelated, then it follows from eq 6 that

$$\sigma_e(t) \cong \frac{3nk_BT}{\nu N_R{}^2 a^2}\langle r^2\rangle P_2 \qquad (9)$$

i.e., in this approximation changes in $\langle r^2\rangle(t;N_R)$ and in $P_2(t;N_R)$ each contribute linearly to the change in $\sigma_e(t)$. The relative changes in these two quantities is shown in Figure 8 for two typical values of N_R.

$\rho = 0.95$. All of the simulation results reported thus far have been for a melt with reduced density of $\rho = 1.0$. To study, in a preliminary way, the effects of this parameter, we have performed a simulation for a somewhat shorter period, of a melt with reduced density $\rho = 0.95$ (packing fraction $\varphi = 0.5$). The four initial configurations for this case are obtained from the corresponding configurations for the melt with $\rho = 1.0$ by subjecting the latter to a slow expansion followed by a brief equilibration period. The initial configurations for $\rho = 0.95$ are, therefore, not independent of those for the $\rho = 1.0$ case, since the large-scale structure of the chains are likely not to have changed significantly. We find that, except for very early time behavior, the

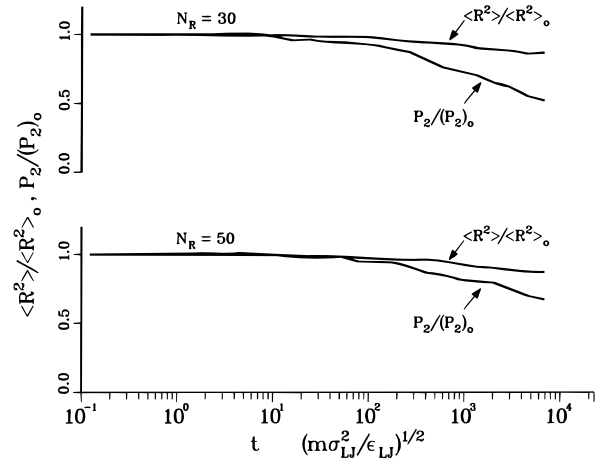

Figure 8. Comparison of decay of end-to-end distance square $\langle r^2\rangle/\langle r^2\rangle_0$ and of orientation $P_2/(P_2)_0$ for segments with $N_R = 30$ and $N_R = 50$ bonds.

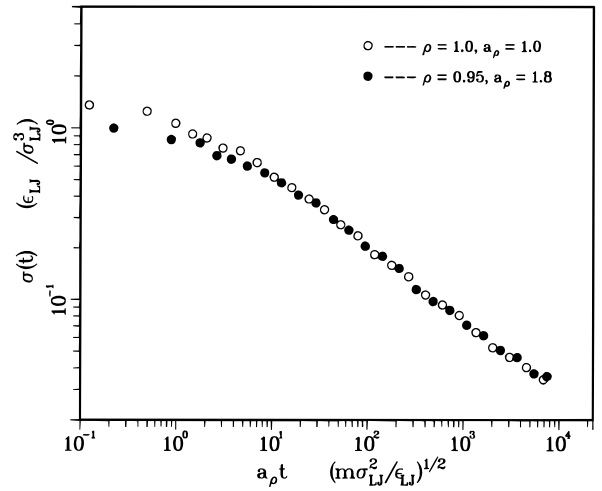

Figure 9. Master curve for stress relaxation $\sigma(t)$ in model polymer melts with reduced densities $\rho = 1.0$ and $\rho = 0.95$ obtained by use of the time-shift factor $a_\rho = 1.8$ for simulation results for $\rho = 0.95$.

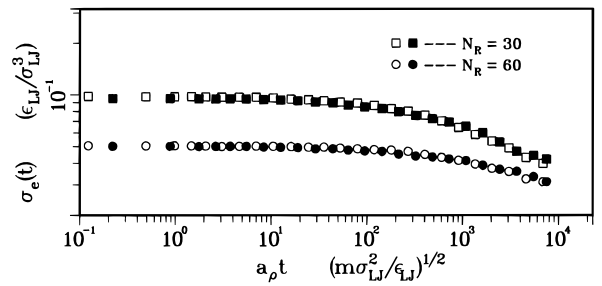

Figure 10. Master curves for entropic stress $\sigma_e(t;N_R)$ for the cases of $N_R = 30$ and 60 bonds per segment and for reduced densities $\rho = 1.0$ (unfilled symbols) and $\rho = 0.95$ (filled symbols). Shift factors a_ρ as in Figure 9.

relation between the results for $\sigma(t)$, $\sigma_e(t;N_R)$, and $P_2(t;N_R)$ can be well represented in terms of a shift factor a_ρ. This is seen in Figures 9 and 10, where a shift factor $a_{0.95} = 1.8$ is employed to bring the results for $\rho = 0.95$ into good coincidence with those for $\rho = 1.0$. The variation along the chain of bond orientation decay for the case of $\rho = 0.95$ is shown in Figure 11. Again, as in the case of $\rho = 1.0$, the rate of decay over the central portion starts to slow down at about $t = 10^2$ (or possibly slightly earlier) relative to the rate of the end portions. However, the results for $\rho = 1.0$ show a greater slowing down at later time for the central portion than do those for $\rho = 0.95$.

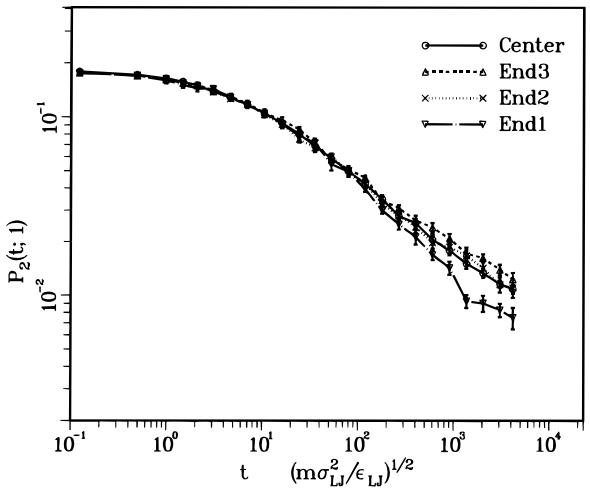

Figure 11. Variation of bond orientation decay along the chains for reduced density $\rho = 0.95$. Definition of chain portions as in Figure 5.

3. Discussion

In this section, we summarize the results of the simulations and discuss some aspects of the stress relaxation process that they illuminate.

Time History. If we base our discussion solely on the stress relaxation history shown in Figure 1, with its accompanying error bars, it is difficult to justify any structure beyond an approximate straight line fit from time $t \sim 10^1$ to the end of the simulation. The following discussion, however, looks ahead to the observed nature of bond orientation decay. This suggests additional structure in the stress relaxation history, which, although not definitely established by the simulation data, appears worthy of study. From this viewpoint, we begin with a discussion of three periods in the early stress relaxation history. The approximate times bounding these periods are for the simulation $\rho = 1.0$.

(a) $t < 10^2$. In this period $\sigma(t) > \sigma_e(t;N_R)$ for all N_R. It is a period of rapid change for $\sigma(t)$; its value declines by almost a decade, to ~0.13 of its initial value. By contrast, the values of $\sigma_e(t;N_R)$ are essentially unchanged for $N_R \geq 30$ and decay only slightly for smaller values of N_R (Figure 2).

(b) $10^2 < t < 2 \times 10^3$. In the graphical representation of Figure 2, we see that in this period the curve of $\sigma(t)$ cuts through the curves of $\sigma_e(t;N_R)$ for different fixed values of N_R. Values of N_R for which there is instantaneous agreement as the curves intersect go from $N_R = 5$ to $N_R = 30$. In this period, $\sigma(t) \sim t^{-0.45}$, to a good approximation as determined by a least-squares fit, while $\sigma_e(t;N_R)$ decay more slowly, at rates that are strongly N_R dependent (Figure 7).

(c) $2 \times 10^3 < t < 7 \times 10^3$ (last data point available from simulation). The value of N_R for which there is instantaneous agreement goes more slowly from $N_R = 30$ to $N_R = 50$. At $t = 2 \times 10^3$ the slope of the $\sigma(t)$ decay appears to change abruptly and in this period $\sigma(t) \sim t^{-0.38}$ as determined by a least-squares fit. There is also an abrupt change in the rate of decay of $\sigma_e(t;N_R)$ near the beginning of this period with the time of the change depending somewhat on N_R; this is seen most clearly in Figure 7. By the end of the simulation at $t \cong 7 \times 10^3$, the value of $\sigma(t)$ has declined to ~0.025 of its initial value.

Bond Orientation Decay. If we turn next to a consideration of the decay in bond orientation as measured by $P_2(t;1)$, Figure 3, we see similar behavior to $\sigma(t)$ in these time periods, with the similarity extend-

ing to details. In particular at $t \cong 2 \times 10^2$ the curve for $P_2(t;1)$ undergoes a transition from smooth decay to one with a small oscillatory or fluctuating component. Examination of $\sigma(t)$ in Figure 1 shows a similar transition, although it is not as easily observed here since $\sigma(t)$ shows greater scatter for $t \lesssim 2 \times 10^2$. At $t \cong 2 \times 10^3$, the curve for $P_2(t;1)$ loses these oscillations and becomes a straight line with reduced slope in complete parallelism to the behavior of $\sigma(t)$.

We may try to correlate these transitions in the behavior of $P_2(t;1)$ with the nature of the decay of bond orientation over the central and over the end portions of the chain in these periods. We see from Figure 5 that for $t \lesssim 10^2$ the decay of bond orientation is uniform over the entire length of the chain. Starting at $t \cong 10^2$, the decay rate over the central portion of the chains starts to slow down relative to the ends, and the decrease in central bond orientation decay becomes even more pronounced in the period $2 \times 10^3 \lesssim t \lesssim 7 \times 10^3$. A similar end effect in decay rates is seen, Figure 6, in the behavior of $\sigma_e(t;N_R)$. This type of orientation and stress decay behavior is, of course, consistent with the onset of reptation at $t \cong 10^2$, although as noted by Lodge *et al.*[16] in connection with variation in the stress relaxation rates along the chains, it does not prove the existence of reptation. Note that we are here using the nature of bond orientation decay rather than the onset of the $t^{1/4}$ regime in the mean square monomer displacement as a measure of reptation; that is, the limiting case of motion of the chain by strict reptation would imply no bond orientation decay over the central portions of the chain until the arrival of the terminal regime.

Finally, we return to a consideration of the decay of $P_2(t;N_R)$ for various values of $N_R \geq 1$ (Figure 3). We find that after the use of suitable vertical scaling factors, the various curves may be superimposed approximately by a time-shift factor, a_{N_R}, where $a_{N_R} \sim N_R^{0.4}$. The orientation of a segment with N_R bonds acts as a topological constraint upon segments with fewer bonds, and the slower decay rates for the larger values of N_R may perhaps provide an example of hierarchical constraints,[28] but we do not pursue this question here.

Atomic vs Molecular Viewpoints. We have been emphasizing two methods of computing stress. The first is the determination of $\sigma(t)$ on the basis of the virial theorem and expressed therefore in terms of atomic interactions, while the second is molecular expressed in terms of the ESSF. The close relation we have observed between the bond orientation decay $P_2(t;1)$ and the stress $\sigma(t)$ is a phenomenon that can only be understood on the atomic level. At later times, $t \lesssim 10^2$, when the ratio $P_2(t;1)/\sigma(t)$ becomes constant, it can be explained in terms of the concept of steric shielding.[29] This term refers to the fact that the interaction between two neighboring atoms or monomers is rendered anisotropic by the shielding from interaction of a given monomer by those bonded to it. When the bond orientation distribution is rendered anisotropic with respect to the laboratory frame by an imposed deformation, so is the stress $\sigma(t)$ due to these interactions. At earlier times there is, besides steric shielding, an additional cause for anisotropic monomer−monomer interaction. This arises from the imposed affine deformation and is the same anisotropy produced in a deformed simple liquid. We may therefore write

$$\sigma(t) = \sigma_{aff}(t) + \sigma_{ss}(t) \tag{10}$$

where σ_{aff} is due to the imposed affine deformation and σ_{ss} is due to steric shielding. The former decays rapidly and is essentially zero in this simulated system by the time $t \cong 10^2$, at which time $P_2(t;1)/\sigma(t)$ reaches its constant value. The latter component, $\sigma_{ss}(t)$, decays more slowly since it depends on decay of the bond orientation, $P_2(t;1)$.

Stress-Optical Coefficient. From the molecular viewpoint, birefringence is discussed in terms of the polarizability of a segment in parallel with the calculation of stress by application of the entropic spring formula to a segment.[30] We have given a framework for the discussion of the stress-optical coefficient on the monomer level.[31] For polymer systems with bond-angle restrictions in the backbone chain, this involves assigning an intrinsic coordinate system to each monomer in which the backbone bonds attached to that monomer are fixed and then expressing both the stress and polarizability tensors with respect to it. This approach utilizes the concept of intrinsic monomer stress[29,32] that plays an important role in the stress relaxation process. Applications of this monomer-level formulation to interpret the experimental behavior of the stress-optical coefficient of various polymers have been made.[33, 34]

For the freely-jointed chain model simulated here, it is not possible to introduce an intrinsic coordinate system for each monomer and to define an intrinsic monomer stress. Nevertheless, as we have seen, it is possible to use the concept of steric shielding (which underlies the nature of the intrinsic monomer stress) and the decomposition of eq 10 to understand the observed behavior of $P_2(t;1)/\sigma(t)$, one which parallels that observed in the stress-optical coefficient generally for real systems as they pass from the glassy to rubbery states.

Rouse Dynamics and Coarse-Graining. The Rouse model[35,36] has been employed in theoretical treatments[3,38] of the period in which transition to the plateau occurs. The application of the Rouse model to a realistic melt model requires coarse-graining of the type we have applied to our idealized model. That is, we break each chain into subchains with N_R bonds each and focus only on the motion of the monomers at the ends of the subchains. The other monomers are not treated explicitly but subsumed into a Rouse segment with each segment regarded as a linear entropic spring. Chain−chain interaction is replaced by a stochastic force and friction constant in a Langevin formulation. With proper choice of the Rouse particle or bead mass and friction constant, it is believed that the motion of the subset of monomers will, in a suitable average sense, have the same motion in the interacting chains of the modeled melt and in the set of independent Rouse chains.[10,14]

The above discussion deals only with monomer dynamics. In the computation of the stresses in the system subsequent to the employment of Rouse dynamics, it is assumed that the same coarse-graining can be employed together with the ESSF of eq 5. This procedure leads to the relaxation modulus $G_R(t)$, where the subscript R denotes that it is computed on the basis of the Rouse model,

$$G_R(t) = \nu k_B T \sum_{p=1}^{N/N_R} \exp(-2tp^2/\tau_R) \tag{11}$$

where N/N_R is the number of Rouse segments per chain and ν is the number of chains per unit volume. At $t = 0$,

$$G_R(0) = \nu(N/N_R)k_B T = ck_B T \tag{12}$$

where c is the number of Rouse segments per unit volume. It is therefore clear from eqs 11 and 12 that the early time behavior of $G_R(t)$ depends sensitively on N_R and, in particular, $G_R(0;N_R) \sim N_R^{-1}$. The stress computed on the basis of the Rouse model, $\sigma_R(t;N_R)$, is linearly proportional to $G_R(t;N_R)$ and, as seen from Figures 2 and 6, the early time behavior of $\sigma_e(t;N_R)$ as determined from the NEMD simulation has the same character as $\sigma_R(t;N_R)$. In fact, in ref 19, it was shown to be possible to fit $\sigma_e(t;N_R)$ for early times by the expression for $\sigma_R(t;N_R)$ based on eq 11. This fit of $\sigma_e(t;N_R)$ to the expression for $\sigma_R(t;N_R)$ failed at longer times in a manner consistent with a transition from Rouse dynamics to that of reptation. Although the Rouse stress $\sigma_R(t;N_R)$ thus appears to have utility as an indicator of the change in character of the dynamics, it must be emphasized that it is a poor representation of stress at early times where $\sigma(t) > \sigma_e(t;N_R)$ for any value of N_R.

The discussion of the Rouse stress given thus far has been based on eq 11. This expression is the rigorous solution for an ensemble of discrete Rouse chains, each with N/N_R Rouse segments and, in particular, the finite character of the sum follows from the finite number of normal modes for such a mechanical system. In the treatment of Doi and Edwards,[3] the discrete Rouse model is replaced by a continuous one, and the upper limit of the sum in eq 11 becomes infinite. In this case, $G'_R(t;N_R)$ where

$$G'_R(t;N_R) = \nu k_B T \sum_{p=1}^{\infty} \exp(-2tp^2/\tau_R) \qquad (13)$$

becomes infinite as $t \to 0$ for any N_R. If we regard the Rouse model as obtained by cross-graining of a real chain, it is clear that there is a lower bound to $N_R = 5$,[27] since each segment must have a sufficient number of persistence lengths to validate its action as a linear entropic spring. It then follows that the infinite sum approximation to eq 10 must be regarded as approximating a very long chain, i.e., $N \to \infty$. However, for any finite N, the limit as $t \to 0$ of $G_R(t;N_R)$, eq 12, depends only on c, the number of Rouse segments per unit volume and is independent of N; the same must then be the case for the limit as $N \to \infty$. Therefore, the behavior of $G'_R(t;N_R)$ is greatly in error at early times and whether $G'_R(t;N_R)$ may be used to determine the plateau modulus G_N° at time $t = \tau_e$ (the time of plateau onset) depends on whether it has become sufficiently accurate by that time. Similar considerations apply to the replacement, for small t, of the infinite sum in eq 11 by an infinite integral leading to the result that $G'_R(t;N_R) \sim t^{-1/2}$, which has been used by Doi and Edwards[3] to relate G_N° to the tube dimensions. From Figure 2 it is seen that the rate of decay of $\sigma_e(t;N_R)$ is substantially slower than $t^{-1/2}$ even for a coarse-graining with $N_R = 5$ (60 segments/per chain). The atomic virial stress on the other hand, which is of course independent of Rouse dynamics, does show a decay behavior in the period $10^2 < t < 2 \times 10^3$ of $\sigma(t) \sim t^{-0.45}$.

To consider the effect of chain tension relaxation prior to plateau onset, Doi and Edwards[3] use a continuous chain formulation for the ESSF, eq 5, in an integral expression that takes the form in present notation[37]

$$t_{ij}^e = \nu \frac{3k_B T}{Na^2} \left\langle \int_0^{L(t)} ds\, L(t) \left(u_i(s,t) u_j(s,t) - \frac{1}{3}\delta_{ij} \right) \right\rangle \qquad (14)$$

where $L(t)$ is the chain contour length and $\mathbf{u}(s,t)$ is the unit vector tangent to the chain at contour distance s. A difficulty with this continuous chain formulation is that it cannot reflect the effect of the parameter N_R upon the time variation of the coarse-grained chain conformation. Doi and Edwards assume that the relaxation of $L(t)$ occurs on the time scale of τ_R, while that of the orientation occurs only on the time scale τ_d, the disentanglement time. On this basis they arrive at the result $G_N^\circ = (4/5)(N/N_e)k_B T$, where N_e is the average number of persistence lengths between entanglements. In our model, however, we find (Figure 3) that, while it is certainly true that chain vector orientation changes take place very slowly, changes in orientation of segments take place on a time scale sensitive to N_R and this change in orientation is, for a range of N_R, much more effective (Figure 8) than the change in segment length in the relaxation of $\sigma_e(t;N_R)$ prior to τ_e.

Comparison with Previous Simulations. The results of the present simulations for a melt of freely-jointed chains with $N = 300$ bonds are similar, in broad outline, with those previously reported[19] for the corresponding melt with $N = 200$. The earlier simulations involved only 1 initial melt configuration rather than the 4 configurations used here and are, therefore, less reliable in details. In both cases the decay of σ(t) shows a slowing down and change of character at comparable times, toward the end of the simulation. For $N = 300$ we saw the change in decay rate from $\sigma(t) \sim t^{-0.45}$ to $\sigma(t) \sim t^{-0.38}$ occurring at $t = 2 \times 10^3$; the earlier $N = 200$ simulation showed an inflection point at $t = 3 \times 10^3$, which we regarded as an incipient plateau. The slowing down and change of character in this time range in the decay of $\sigma_e(t;N_R)$ are, perhaps, clearer than for $\sigma(t)$ and are also seen in both simulations. (See Figure 7 in this paper and Figure 6 in ref 19.) In the simulation for $N = 200$, we found $\sigma(t) = \sigma_e(t;40)$ for the period after the inflection point at $t = 3 \times 10^3$ until the end of the simulation at $t = 10^4$. There is no such period for which $\sigma(t) = \sigma_e(t;N_R)$ for any fixed value of N_R observed in the present simulation for $N = 300$. Further simulations will be needed to determine if these differences are due to statistical fluctuations or represent actual differences in the behavior of this model for $N = 200$ and $N = 300$.

The times at which we observe a slowing down in the rate of decay of $\sigma(t)$ for $N = 300$ ($t \cong 2 \times 10^3$) or an inflection point for $N = 200$ ($t \cong 3 \times 10^3$) compare well with the estimates of the entanglement time τ_e made on the basis of equilibrium simulations ($\tau_e \cong 2 \times 10^3$ in ref 10 and $\tau_e \cong 10^3$ in ref 15). If we turn attention to bond orientation, we observe that the rate of bond orientation decay over the central and end portions of the chains in our simulations for $N = 300$, $\rho = 1.0$, start to show a difference as early as $t \cong 2 \times 10^2$, although a distinct slowing down of this decay over the central portion does not take place until $t \cong 3 \times 10^3$ (Figure 5). These results on bond orientation decay are consistent in a general way with the decline in the rate of growth of mean square displacements of the central portion of the chain observed in other computer simulations.[10,12]

4. Conclusions

The physical picture underlying the stress in a deformed crystalline solid is relatively straightforward. Atoms remain in the vicinity of lattice sites and the stress arising from a deformation may be understood in terms of the change in atom interaction energy due to changes in interatomic distances. Thermal motion of the atoms plays only a minor role.[39]

In a liquid-like system such as a polymer melt, on the other hand, thermal motion causes atoms to move large

distances in macroscopic time intervals, and it is necessary to speak of statistical descriptions of atom positions using the language of probability distributions. Macroscopic deformations render these distributions anisotropic, thus giving rise, through the virial stress formula, to anisotropic or deviatoric stresses. (The existence of anisotropic stresses immediately after the imposition of an appropriate macroscopic deformation, in fact, demonstrates the anisotropy of these distributions.)In this paper we have considered partial descriptions of the distribution anisotropy through the quantities we have denoted by $P_2(t;N_R)$. For $N_R = 1$, $P_2(t;1)$ is a measure of orientation of the individual bonds of our chain model, while for $N_R > 1$ they describe orientation of the corresponding segments. Although we did not compute it in our simulations, it is also helpful to consider $P_2(t;0)$, which is an orientation measure of the vectors $\mathbf{r}_\alpha(t)$ connecting nonbonded interacting pairs. Our simulations show that immediately after deformation, at time $t = 0+$, all of these measures $P_2(0+;N_R)$, $N_R > 0$, are nonzero due to the affine deformation, and we conjecture that the same is true for $P_2(0+;0)$. These orientation measures then decay, with relaxation times that increase with N_R. Presumably, for very long times, all have decayed to negligible values except $P_2(t;N)$, the chain vector orientation measure, and τ_N then governs the terminal rate of stress relaxation. For earlier times, however, $P_2(t;N_R)$ with small N_R play important roles. Immediately after loading, in the glassy period, we expect that $P_2(t;0)$ plays the major role giving rise to what we have termed σ_{aff}. When $P_2(t;0)$ and σ_{aff} decay to negligible values, $P_2(t;1)$ becomes important. In our simulations, the decay to zero of σ_{aff} occurs at $t \cong 10^2$, as seen most clearly from the ratio of $P_2(t;1)/\sigma(t)$ shown in Figure 4. What is unexpected and important is that this ratio is constant (within statistical fluctuations) for $t \gtrsim 10^2$, so that the deviatoric stress $\sigma(t)$ can be regarded then as determined by the bond orientation $P_2(t;1)$. This result, difficult to rationalize on the molecular level, can be understood on the atomic level in terms of the mechanism of steric shielding and, for chains with fixed bond angles, is closely relative to the concept of intrinsic monomer stress[29,32] and the monomer-level description of the stress-optical coefficient.[31]

Some further conclusions from the present simulations are as follows:

Bond orientation decay over the central portion of the chain for the case of $\rho = 1.0$ shows a distinct slowing down at $t \cong 3 \times 10^3$; this behavior is consistent with an onset of reptation at this time.

There are conceptual difficulties with the use of Rouse dynamics in the transition period for the computation of the plateau modulus G_N^0.

In a recent paper, Antonietti *et al.*[40] have described viscoelastic experiments on a new polymer system of small spherical polystyrene microgels which they describe as "rubbery nanospheres." Although the chain topology is very different, its viscoelastic response for appropriate conditions exhibits a plateau and plateau modulus very like that for a linear chain system with much lower molecular weight. The similarity in behavior for very different chain topology suggests that, although topology must play a critical role in determining the time scale, an atomistic viewpoint may be valuable in understanding some of the general features of this process.

Acknowledgment. This work was supported by the Gas Research Institute (Contract No. 5091-260-2237) with the computations performed on the Cray C-90 at the Pittsburgh Supercomputing Center. We thank Dr. George Loriot for advice and assistance in postprocessing of data.

References and Notes

(1) de Gennes, P.-G. *J. Chem. Phys.* **1971**, *52*, 572.
(2) Doi, M.; Edwards, S. F. *J. Chem. Soc., Faraday Trans. 2* **1978**, *74*, 1789, 1802, 1818.
(3) Doi, M.; Edwards, S. F. *The Theory of Polymer Dynamics*; Clarendon Press: Oxford, UK, 1986.
(4) Richter, D.; Butera, R.; Fetters, L. J.; Huang, J. S.; Farago, B.; Ewen, B. *Macromolecules* **1992**, *25*, 6156.
(5) Ewen, B.; Maschke, U.; Richter, D.; Farago, B. *Acta Polym.* **1994**, *45*, 143.
(6) Richter, D.; Willner, L.; Zirkel, A.; Farago, B.; Fetters, L. J.; Huang, J. *Macromolecules* **1994**, *27*, 7437.
(7) Perkins, T. T.; Smith, D. E.; Chu, S. *Science* **1994**, *264*, 819.
(8) Kas, J.; Strey, H.; Sackmann, E. *Nature* **1994**, *368*, 226.
(9) Kolinski, A.; Skolnick, J.; Yaris, R. *J. Chem. Phys.* **1987**, *86*, 1567, 7164, 7174.
(10) Kremer, K.; Grest, G. *J. Chem. Phys.* **1990**, *92*, 5057.
(11) Kolinski, A.; Skolnick, J. *J. Phys. Chem.* **1993**, *97*, 3450.
(12) Ngai, K. L.; Peng, S. L.; Skolnick, J. *Macromolecules* **1992**, *25*, 2184.
(13) Shaffer, J. S. *J. Chem. Phys.* **1995**, *103*, 761.
(14) Smith, S. W.; Hall, C. K.; Freeman, B. D. *Phys. Rev. Lett.* **1995**, *75*, 1316.
(15) Smith, S. W.; Hall, C. K.; Freeman, B. D. *J. Chem. Phys.* **1996**, *104*, 5616.
(16) Lodge, T. P.; Rotstein, N.; Prager, S. *Adv. Chem. Phys.* **1990**, *79*, 1.
(17) Gao, J.; Weiner, J. H. *Macromolecules* **1992**, *25*, 1348, 3462.
(18) Gao, J.; Weiner, J. H. *J. Chem. Phys.* **1992**, *97*, 8698.
(19) Gao, J.; Weiner, J. H. *J. Chem. Phys.* **1995**, *103*, 1614, 1621.
(20) Gao, J.; Weiner, J. H. *Macromolecules* **1989**, *22*, 979.
(21) Fixman, M. *J. Chem. Phys.* **1991**, *95*, 1410.
(22) Takeuchi, H.; Roe, R.-J. *J. Chem. Phys.* **1991**, *94*, 7446, 7458.
(23) Gao, J.; Weiner, J. H. *J. Chem. Phys.* **1993**, *98*, 8256.
(24) Gao, J. *J. Chem. Phys.* **1995**, *102*, 1074.
(25) The subscript R in ν_R and N_R denotes Rouse since we use the same coarse-graining in our discussion of the use of Rouse dynamics that appears later. It should be emphasized, however, that in the present use of the ESSF leading to $\sigma_e(t)$ through eq 6, the required segment dynamics, $\mathbf{r}_\beta(t)$, are determined from the molecular dynamics of the full interacting system and not through the dynamics of the Rouse model.
(26) See, for example, ref 3, p 220, or ref 16, p 24.
(27) Weiner, J. H., *Statistical Mechanics of Elasticity*; Wiley: New York, 1983. See p 241 ($N_R = 2$), p 242 (($N_R = 3,4$), and p 247 ($N_R = 5$).
(28) Palmer R. G.; Stein, D. L.; Abrahams, E.; Anderson, P. W. *Phys. Rev. Lett.* **1984**, *53*, 958.
(29) Gao, J. G.; Weiner, J. H. *Science* **1994**, *266*, 748.
(30) See, for example: Flory, P. J. *Statistical Mechanics of Chain Molecules*; Interscience: New York, 1969; Chapter IX. Mattice, W. L.; Suter, U. W. *Conformational Theory of Large Molecules*; J Wiley: New York, 1994; Chapter XIV.
(31) Gao, J.; Weiner, J. H. *Macromolecules* **1994**, *27*, 1201.
(32) Gao, J.; Weiner, J. H. *J. Chem. Phys.* **1989**, *90*, 6744.
(33) Osaki, K.; Okamoto, H.; Inoue, T.; Hwang, E.-J. *Macromolecules* **1995**, *28*, 3625.
(34) Okamoto, H.; Inoue, T.; Osaki, K. *J. Polym. Sci., Part B: Polym. Phys.* **1995**, *33*, 1409.
(35) Rouse, P. E. *J. Chem. Phys.* **1953**, *21*, 1272.
(36) Bueche, F. *J. Chem. Phys.* **1954**, *22*, 603.
(37) Reference 3, p 244
(38) Ferry, J. D. *Viscoelastic Properties of Polymers*, 3rd ed.; Wiley: New York, 1980.
(39) See, for example, reference 27, Chapter 4.
(40) Antonietti, M.; Pakula, T.; Bremser, W. *Macromolecules* **1995**, *28*, 4227.

MA9602177